JOURNAL OF SPACECRAFT AND ROCKETS
Vol. 43, No. 2, March–April 2006

Low-Thrust Spacecraft Formation Keeping

Pierre Vignal* and Henry Pernicka†
University of Missouri–Rolla, Rolla, Missouri 65409-0050

Replacing large and costly satellites with formations of smaller satellites, flying in close proximity, is a current subject of interest. One of the keys to successful formation flying is the control system that maintains the formation geometry and provides proper positioning of each member of the formation. This study compares two active control system designs that can be used to maintain a formation composed of microsatellites with limited on-off thrusting capabilities in low Earth orbit. The two evaluated designs are based on a linear approach using optimal control theory and on a nonlinear approach based on Lyapunov stability concepts. In assessing the effectiveness of each controller, the performance criteria were the accuracy with which the formation is maintained and the propellant consumption. The final selection is a tradeoff between fuel consumption and controller robustness based on model uncertainties.

Nomenclature

a_{mrs}	=	semimajor axis of leader orbit
$\boldsymbol{Co}$	=	controllability matrix
$\boldsymbol{e}_3$	=	unit vector fixed in the Earth along the direction of the north pole axis
F_x, F_y, F_z	=	components of the control force along the rotating x, y, and z axes, respectively
$\boldsymbol{f}$	=	control force vector (force applied by the onboard propulsion system)
J	=	cost function associated with the optimal control
J_2	=	Earth oblateness harmonic coefficient
K_{global}, K_P, K_D	=	positive gains associated with the nonlinear controller
m	=	mass of the spacecraft
$\boldsymbol{P}$	=	unique positive definite solution of the algebraic matrix Riccati equation
$\boldsymbol{Q}$	=	matrix associated with the states (for the linear quadratic regulator controller)
$\boldsymbol{R}$	=	matrix associated with the input (for the linear quadratic regulator controller)
R_{Earth}	=	Earth radius
r	=	magnitude of the $\boldsymbol{r}$ vector
$\boldsymbol{r}$	=	position vector of spacecraft in the terrestrial frame
r_{amr}	=	apogee of follower's original orbit
r_{pmrs}	=	perigee of leader's orbit
T	=	constant thrust level of the engine
$\boldsymbol{u}$	=	command vector
V	=	Lyapunov function
$\boldsymbol{v}$	=	velocity vector of spacecraft in the terrestrial frame
$\boldsymbol{X}$	=	state vector
x, y, z	=	components of follower relative position vector with respect to leader (in the Linear Controller section); components of each spacecraft position vector in the terrestrial frame (in the Nonlinear Controller section)
μ_{Earth}	=	Earth's gravitational parameter, taken as 398,600 km^3/s^2
ρ	=	scalar control weighting factor on the thrust (linear controller)
σ_D	=	scalar weighting factor associated with the relative position (linear controller)
σ_V	=	scalar weighting factor associated with the relative velocity (linear controller)
ω	=	leader's angular velocity magnitude in the terrestrial frame

Presented as Paper 2004-296 at the AAS/AIAA 14th Space Flight Mechanics Meeting, Maui, HI, 8–12 February 2004; received 26 May 2004; revision received 6 April 2005; accepted for publication 12 April 2005.

*Graduate Student, Department of Mechanical and Aerospace Engineering, 1870 Miner Circle; pierrevignal@yahoo.fr. Member AIAA.

†Associate Professor, Department of Mechanical and Aerospace Engineering, 1870 Miner Circle; pernicka@umr.edu. Senior Member AIAA.

Introduction

RECENT years have seen significant interest in mission architectures using formations of spacecraft. The advantages of flying spacecraft in formations are now well known. Many studies in the open literature regarding formation flight have been published, and a few are given here.[1–9] In this study, formation flight is considered for the case in which only very limited on-off thrusting capability is available onboard the spacecraft. Two candidate controller designs are evaluated, one based on a linear approach using optimal control theory and the other on a nonlinear approach based on Lyapunov stability concepts. In assessing the effectiveness of each controller, the performance criteria were the accuracy with which the formation is maintained and the propellant consumption. The final selection is a tradeoff between fuel consumption and controller robustness based on model uncertainties. The spacecraft formation in this study (a leader–follower configuration) is controlled to a "short" 10-m range, much less than most formations considered in the open literature.

This study also presents a bielliptic transfer specifically designed to allow the formation pair to reconfigure from its original tethered geometry in a manner that allows the spacecraft pair to remain in continuous radio contact.

The motivation of this work originated with the MR SAT mission, currently under development at the University of Missouri–Rolla. Because of the requirement to use an off-the-shelf intersatellite communication system, an autonomous algorithm that provides a recovery system for the formation should the intersatellite communication system fail was developed. Similar algorithms could be adopted for use with other formation missions as part of a mission "safe mode."

In examining related previous studies in the open literature, only works involving formation flying were considered in detail in order to facilitate comparison of the presented results to previously published data. In examining the various methods that have been used or are currently in use in satellite guidance systems, a controller based on linearizing the equations of motion is common. Although this method was developed for docking sequences in space, the Clohessy–Wiltshire linearization is frequently found in guidance problems.[1–5] However, different methods are then chosen to compute the gains of the systems. Among these methods, the following

can be found: 1) classical proportional-integral-derivative controller, 2) optimal control based on linear-quadratic-regulation (LQR) control, 3) H-infinity control, and 4) optimal control based on neural-network techniques.

Linearization of the equations of motion is commonly used in satellite guidance systems and provides good performance in terms of tracking error and overall propellant consumption. A limitation of linearization techniques is that orbital dynamics involve highly nonlinear differential equations. As a given linearization is only valid around a reference solution, to properly design a linear controller to stabilize a nonlinear system, the entire trajectory must be subdivided in smaller segments. This leads to several linearizations that are only valid near their reference solutions. For highly nonlinear systems, the number of segments might be very large, requiring the definition of a large number of separate controllers. Such systems require significant onboard memory to store the parameters that define each controller.

Regarding optimal control approaches, one limitation derives from the robustness of these controllers. Optimal controllers are designed for specific dynamics. If the dynamics of the system changes, the controller is no longer optimal and might not even be stable. The robustness of the designed controller must be tested before a final selection is made. These two limitations led to the consideration of another type of controller based on nonlinear techniques based on Lyapunov stability concepts. Properly designed nonlinear controllers are not restricted to stability consideration over a specific trajectory segment that linear controllers are restricted to and remain valid on the entire trajectory. This characteristic promotes the robustness of the control system. These nonlinear methods have been developed to increase the robustness of the control system and guarantee stability on a larger set. A secondary reason for the introduction of nonlinear techniques is to increase the performance of the system by having a better prediction of the system behavior. The Clohessy–Wiltshire (C-W) linearization assumes near-circular orbits, and only the Earth's spherical gravitational effect is included in the controller. Significant perturbations such as Earth's geopotential, solar radiation pressure, atmospheric drag, and solar and lunar gravity fields are not included in the controller. For missions that require an extremely high level of accuracy, the Clohessy–Wiltshire linearization technique might not stabilize the considered system. For these types of missions, nonlinear techniques have been developed based on Lyapunov theories. Depending on the level of accuracy required, various types of perturbations can be implemented in the designed controller. A large class of studies[6,7,8,10] has shown that controllers based on Lyapunov theories can be developed for maintaining Earth orbiters as well as for formation-keeping procedures.

With the preceding in mind, two following candidate control laws were studied: 1) a Clohessy–Wiltshire linearization coupled to optimal LQR control and 2) a nonlinear approach based on Lyapunov theories.

As already mentioned, several techniques can be used to define the set of parameters of a linearized system. Although Gurfil et al.[9] showed that neural-network techniques outperform LQR techniques in terms of accuracy, the LQR control technique was chosen here to define the set of parameters of the C-W linearization. Regarding this LQR controller, a similar approach to the one developed by Starin et al.[2,3] was studied. However, unlike in Starin's work, the radial input here is not restricted, and full three-dimensional thrusting is allowed by the control system.

As also mentioned earlier, several nonlinear controllers based on Lyapunov stability concepts have been developed for satellite formation-keeping purposes. The nonlinear controller described in this paper is similar to the one developed by Wang et al.[7] associated with state feedback techniques but with very different constraints. In Wang's paper, variable thrust was applied (whereas the controller here is restricted to low levels of constant on-off thrust), and thrust level was not limited. The maximum thrust level required to achieve a 10-m separation in Wang's paper was up to four times the level used in this paper (12 vs 3 mn).

Another nonlinear controller similar to the one presented in this paper was developed by Yan et al.[6] and applied to formation-keeping procedures in low Earth orbit. The purpose of this controller was to guarantee global uniform ultimate boundedness by developing a Lyapunov-based nonlinear output feedback law controller. Yan's design achieves high formation accuracy with low thrust capabilities. However, it was applied to a large spacecraft (initial spacecraft mass of 1550 kg, final mass of 410 kg), whereas this study focuses on microsatellite applications.

More sophisticated nonlinear controllers were developed by Nelson et al.[10] for low-Earth-orbit applications in order to optimize propellant consumption. These controllers were based on sliding-mode control theories associated with simple linear Hill's equations in order to describe the motion of each spacecraft of the formation. By applying decentralized commands, Nelson was able to reduce the propellant consumption and to take advantage of the "good" dynamics that do not break the formation geometry. At this time, only preliminary work has been done to implement similar concepts to the controller considered here, and the nonlinear controller presented in this paper does not yet include these improvements.

The Lyapunov controller described here is based on a study previously given by Naasz,[8] which consists of generating a Lyapunov function that models the system (satellite formation in low Earth orbit with limited thrust) and applying feedback linearization techniques to generate the control command. The approach presented in this study extends Naasz's work by following one of his recommendations: Naasz only includes the spherical gravitational effect and recommends including the J_2 effect as well. This recommendation is motivated by the fact that J_2 is the second largest contribution to the acceleration after the spherical gravitational force. Accordingly, this effect has been included in the Lyapunov controller developed in this work.

MR SAT Overview

Students, faculty, and staff at the University of Missouri–Rolla are designing and building a pair of tethered microsatellites as both a research and an educational endeavor. This project is designated as the MR SAT Project (Missouri–Rolla Satellite) and is composed of two spacecraft linked to each other with a 10-m-long tether. The two main mission objectives are to 1) demonstrate the concept of satellites flying in close formation with and without a tether and 2) demonstrate the viability of establishing a communication network between two or more spacecraft based on low-cost off-the-shelf 802.11 technologies. (The 802.11 standard is an Institute of Electrical and Electronics Engineers standard defining wireless network protocol and hardware specifications. It is the main protocol used today in wireless applications and is also known as "WiFi.")

Figure 1 shows a three-dimensional representation of MR SAT. The primary spacecraft, MR SAT, has an approximate mass of 20 kg and is cube shaped with dimensions $45 \times 45 \times 45$ cm. The secondary spacecraft has an approximate mass of 5 kg with dimensions $30 \times 30 \times 13$ cm, and it is designated MRS SAT (Missouri–Rolla

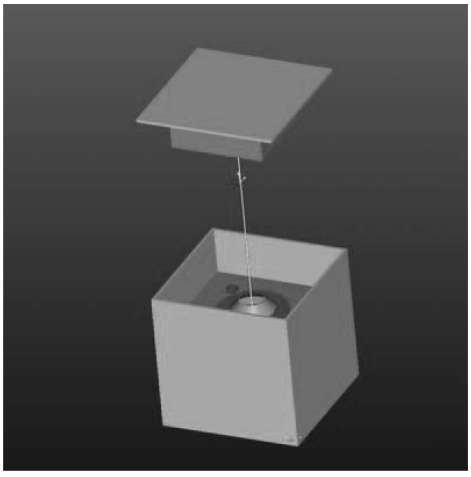

Fig. 1 MR SAT and MRS SAT.

Second Satellite). At launch, MRS SAT is docked to MR SAT. Once on orbit MR SAT and MRS SAT are separated by the 10-m tether. After flying in the tethered formation for a predetermined time period, the spacecraft will free fly when the tether is (intentionally) released. MR SAT will then attempt to maintain formation with the passive MRS SAT using limited onboard thrusting capability. In the MR SAT mission only two satellites will compose the formation, but the concepts presented can also apply to larger formations.

Formation-Keeping Objectives

The focus of this paper is on the formation-keeping "chasing" process that occurs during the last phase of the mission. The main objectives are to 1) maintain a close formation between the leader/follower (MRS SAT/MR SAT) within a 10-m radius and 2) control the relative position of the follower within plus or minus 1 m of the nominal 10-m separation. Both objectives are to be met with only limited thrusting available aboard the follower spacecraft, as described in the next section.

Chasing Process Constraints

Because of size, mass, and budget limitations, tradeoffs were made on several key elements that led to specific technical choices. The limitations that affect the chasing process concern the propulsion, communication, and attitude subsystems.

Propulsion Limitations

The follower will be equipped with a set of thrusters; however, the leader is assumed to not be able to perform any orbital maneuvers and is considered a completely passive vehicle. Without an onboard propulsion system, the leader will only control its attitude, leaving its orbit free to drift. The cold-gas propulsion system onboard the follower is assumed to have the following characteristics: 1) a total thrust magnitude of 3.062 mn, 2) firing capabilities in three dimensions, 3) constant fuel flow rate of 4.712×10^{-6} kg/s (on–off engine), and 4) specific impulse I_{sp} of 66 s. (The second assumption requires that a number of thrusters be used on the follower. Such an arrangement will require higher propellant consumption because of the inefficiency encountered in using combinations of thrusters to provide an impulse along the desired direction.)

The quantity of onboard propellant is assumed to be one liter of liquid butane with mass approximately 605 g. Based on the characteristics of the propulsion system just described, the total burn time is equal to 35.676 h.

Data-Acquisition Limitations

To design a control system, the controller's input data must be defined. In the case of a chasing process, the controller requires frequent updating of the relative position vector and the relative velocity vector between the two spacecraft. Both satellites are assumed to be equipped with onboard global-positioning-system (GPS) receivers and intersatellite transceivers. Positions and velocities will be determined using onboard GPS receivers, and leader data will be transmitted to the follower through the intersatellite link. The follower onboard computer will then provide the required information to the controller. Thus it is critical to maintain radio contact during the entire mission. In the case of loss of radio contact, the closed-loop system will not function, and the position of the follower could not be controlled, which could possibly lead to a collision or the leader drifting out of the range of the intersatellite communication link. Radio contact is assumed lost when the distance between the two spacecraft exceeds approximately 460 m.

Tether Release Conditions

At the conclusion of the previous phase of the mission during which close formation flight with the tether attached is studied and demonstrated, the leader/follower center of mass will be moving on a near-circular orbit, and the tether will be aligned with the center of the Earth as a result of the gravity-gradient effect. While tethered, an initial altitude of 700 km and initial inclination of 56 deg was assumed for the leader/follower center of mass. The longitude of the ascending node and the argument of periapsis were arbitrarily set to zero for computational convenience. The two satellites will rotate with the same angular velocity because of the tether constraint. This equal angular velocity will create slightly different translational velocities because the two spacecraft will not be flying at the same altitude. When the tether is released, the angular velocity constraint will disappear. Thus, at $t = 0$ (tether release time) the follower will be located at its apogee, and its velocity will start increasing, and the leader will be at its perigee, and its velocity will start decreasing. Note that because of the assumed short 10-m tether the eccentricities of the leader/follower orbits will be extremely small, and the satellite trajectories will be nearly circular. Specifically, at tether release the eccentricities of the follower and leader will be 0.106×10^{-5} and 0.318×10^{-5}, respectively. Immediately following tether release, a bielliptic transfer is initiated by the follower to place it 10 m behind the leader on the same orbit. This transfer is described in detail in the next section.

Initial Orbit Transfer

Purpose of the Transfer

The purpose of the initial transfer is to relocate the follower on the leader's orbit to simplify the chasing process. (Otherwise at tether release, the spacecraft pair will quickly drift apart because their orbital altitudes are different.) The overall transfer duration will require 5926 s (approximately 99 min), which corresponds to one orbital period for the leader. Impulsive thrusting will be used to perform the required burns, and all of the associated parameters will be computed on Earth prior to launch and stored in the onboard computer database (but these parameters will be able to be updated based on current orbit determination data). However, on "final approach" a controller is required to achieve the final 10-m separation between the spacecraft with sufficient precision. In this regard, when the follower is approximately 5 m away from the leader (which corresponds to 5500 s after the initial burn), the closed-loop controller will be activated. The active system will be turned on to avoid a collision and place the follower 10 m from the leader. Activation of the control system is required as the transfer (described next) is designed to rendezvous with the leader (as opposed to terminating at the required 10-m separation between the two spacecraft). Activating the control system at 5 m was an arbitrary choice, and future efforts will refine this value.

Architecture and Parameters of the Transfer

A simple bielliptic transfer maneuver was selected in part to reduce the distance between the two spacecraft during the maneuver so that radio contact is maintained. The overall transfer is defined by a single parameter: the apogee of the intermediate orbit [defined as r_a in Eq. (1)]. This parameter facilitates the design of the timing of the transfer such that the two spacecraft rendezvous, in contrast to the more obvious Hohmann-transfer choice. If a Hohmann transfer were used, the fixed time of flight would not allow the spacecraft to rendezvous (the leader would have drifted "behind" the follower at the conclusion of the Hohmann transfer). To compute the apogee of the bielliptic transfer, the duration of the two half-ellipses that compose the transfer was set equal to the duration of one leader period. This statement can be mathematically expressed as

$$2\pi\sqrt{\frac{a_{\text{mrs}}^3}{\mu_{\text{earth}}}} = \pi\sqrt{\frac{[0.5(r_{\text{amr}} + r_a)]^3}{\mu_{\text{earth}}}} + \pi\sqrt{\frac{[0.5(r_{\text{pmrs}} + r_a)]^3}{\mu_{\text{earth}}}} \quad (1)$$

Equation (1) was solved numerically using the MAPLE software application. It has three distinct solutions but only one real root (the two other are complex conjugates). Therefore, only one value of r_a is possible and was determined as 7078.06 km. The next step was to compute the ΔV needed from each burn, which are determined as follows:

Burn 1: $\Delta V = 19.87$ mm/s at $t = 0$ s.

Burn 2: $\Delta V = 2.65$ mm/s at $t = 2963$ s.

Burn 3: $\Delta V = -1.34$ mm/s (in the opposite direction of the arrival velocity) at $t = 5926$ s. The trajectories of the spacecraft during the transfer along with the corresponding burns are presented in Fig. 2.

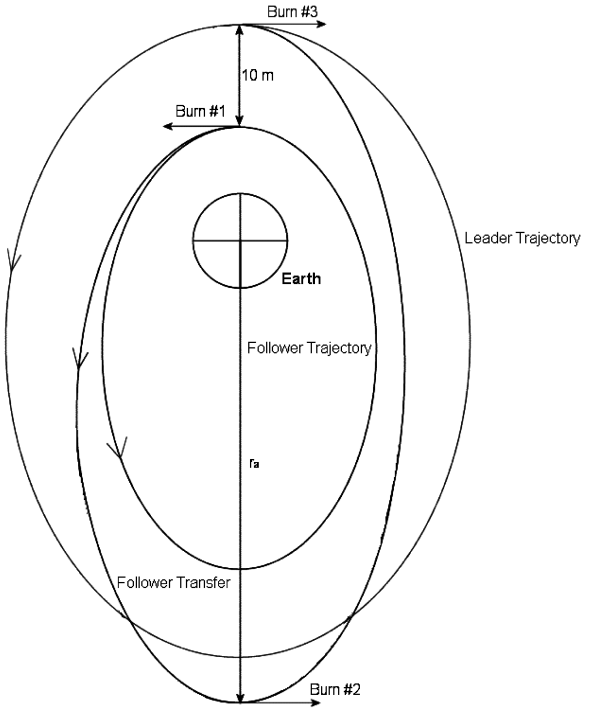

Fig. 2 Follower and leader trajectories during the initial transfer (not to scale).

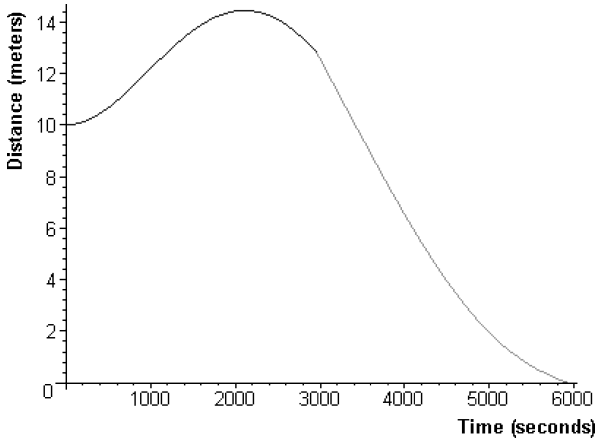

Fig. 3 History of the distance between the follower and the leader during the initial transfer.

Figure 3 shows the history of the distance between the spacecraft during the transfer. On this figure, the activation of the controller has not been taken into consideration, which is why the final distance is zero (and not 10 m). Note that the history of the distance between the spacecraft presented in Fig. 3 was computed using a simple model with no perturbations included.

This figure clearly demonstrates that the intersatellite communication link will not be lost during the initial transfer as the maximum distance between the two spacecraft only reaches 14 m.

As mentioned earlier in this section, the closed-loop controller will be activated before the follower actually rendezvous (collides) with the leader. Thus burn 3 of the bielliptic transfer will not be performed. Instead, the chasing control procedure will be activated. To observe the transition from the unguided mode (open loop) to the fully guided mode (closed loop), the entire transfer was simulated using a MATLAB® simulation (described later in the Simulator Architecture section). The outcome of these simulations is presented in the Results section.

Candidate Controllers

Clohessy–Wiltshire Linearization

To compute a gain matrix that will stabilize the system, the familiar Clohessy–Wiltshire equations are used to define the dynamics of the two spacecraft as

$$\begin{bmatrix} \ddot{x} - 2\omega\dot{y} = F_x \\ \ddot{y} + 2\omega\dot{x} - 3\omega^2 y = F_y \\ \ddot{z} + \omega^2 z = F_z \end{bmatrix} \tag{2}$$

Note that this controller takes only into consideration the spherical gravitational force and that no perturbations are included. It is assumed that both satellites have a circular motion (which is valid because both orbits will have small eccentricities).

The dynamics of the system can be described with the simple linear expression

$$\dot{\boldsymbol{X}}(t) = \boldsymbol{A}\boldsymbol{X}(t) + \boldsymbol{B}\boldsymbol{u}(t) \tag{3}$$

where

$$\boldsymbol{X}(t) = [x(t) \quad y(t) \quad z(t) \quad \dot{x}(t) \quad \dot{y}(t) \quad \dot{z}(t)]^T \tag{4a}$$

$$\boldsymbol{u}(t) = [F_x(t) \quad F_y(t) \quad F_z(t)]^T \tag{4b}$$

$$\boldsymbol{A} = \begin{bmatrix} 0 & 0 & 0 & 1 & 0 & 0 \\ 0 & 0 & 0 & 0 & 1 & 0 \\ 0 & 0 & 0 & 0 & 0 & 1 \\ 0 & 0 & 0 & 0 & 2\omega & 0 \\ 0 & 3\omega^2 & 0 & -2\omega & 0 & 0 \\ 0 & 0 & -\omega^2 & 0 & 0 & 0 \end{bmatrix} \tag{4c}$$

$$\boldsymbol{B} = \begin{bmatrix} 0 & 0 & 0 \\ 0 & 0 & 0 \\ 0 & 0 & 0 \\ 1 & 0 & 0 \\ 0 & 1 & 0 \\ 0 & 0 & 1 \end{bmatrix} \tag{4d}$$

Linear-Quadratic-Regulator Controller

Standard optimization techniques can then be used to stabilize the linearized system and compute the required gains. For this study an optimal LQR approach was selected. The response of the controller is a compromise between fuel consumption and performance. As the follower is assumed to be equipped with on-off engines, the cost function is expressed by the duration of the thrusting burn. The shorter this duration, the lower the propellant consumption. This optimization can be represented by the cost function

$$J = \int_{\theta o}^{\infty} (\boldsymbol{X}^T \boldsymbol{Q}\boldsymbol{X} + \boldsymbol{u}^T \boldsymbol{R}\boldsymbol{u})\, \mathrm{d}\theta \tag{5}$$

The optimal controller is given by

$$\boldsymbol{u}(\boldsymbol{t}) = -\boldsymbol{K}\boldsymbol{X}(\boldsymbol{t}) \tag{6}$$

The optimal feedback gain matrix $\boldsymbol{K}$ is given by

$$\boldsymbol{K} = \boldsymbol{R}^{-1}\boldsymbol{B}^T\boldsymbol{P} \tag{7}$$

where $\boldsymbol{P} > 0$ is the unique positive-definite solution of the algebraic matrix Riccati equation:

$$\boldsymbol{A}^T\boldsymbol{P} + \boldsymbol{P}\boldsymbol{A} - \boldsymbol{P}\boldsymbol{B}\boldsymbol{R}^{-1}\boldsymbol{B}^T\boldsymbol{P} + \boldsymbol{Q} = 0 \tag{8}$$

The cost matrices $\boldsymbol{R}$ and $\boldsymbol{Q}$ associated with the input and the states, respectively, are defined as

$$\boldsymbol{R} = \begin{bmatrix} \rho & 0 & 0 \\ 0 & \rho & 0 \\ 0 & 0 & \rho \end{bmatrix}, \qquad \boldsymbol{Q} = \begin{bmatrix} \sigma_D & 0 & 0 & 0 & 0 & 0 \\ 0 & \sigma_D & 0 & 0 & 0 & 0 \\ 0 & 0 & \sigma_D & 0 & 0 & 0 \\ 0 & 0 & 0 & \sigma_V & 0 & 0 \\ 0 & 0 & 0 & 0 & \sigma_V & 0 \\ 0 & 0 & 0 & 0 & 0 & \sigma_V \end{bmatrix}$$

Stability Check

The controlled system must conform to certain criteria to guarantee stability. Several authors[2,3,5] have previously shown that the linear-quadratic-regulation method applied to a linearized system meets these criteria. To apply the LQR method, the system must meet the following criteria: 1) the pair $(\boldsymbol{A}, \boldsymbol{B})$ is stabilizable; 2) $\boldsymbol{R}$ is positive definite ($\boldsymbol{R} > 0$); 3) $\boldsymbol{Q}$ is positive semidefinite ($\boldsymbol{Q} \geq 0$); and 4) $(\boldsymbol{Q}, \boldsymbol{A})$ has no unobservable poles on the imaginary axis.

To verify that the pair $(\boldsymbol{A}, \boldsymbol{B})$ is stabilizable, the corresponding controllability matrix $\boldsymbol{Co}$ must be computed. This matrix is defined by the expression

$$\boldsymbol{Co} = [\boldsymbol{B} \quad \boldsymbol{AB} \quad \boldsymbol{A}^2\boldsymbol{B} \quad \cdots \quad \boldsymbol{A}^{n-1}\boldsymbol{B}] \tag{9}$$

where the dimension of $\boldsymbol{A}$ is $n \times n$.

The pair $(\boldsymbol{A}, \boldsymbol{B})$ is stabilizable if the rank of its controllability matrix is equal to the dimension of $\boldsymbol{A}$. The MATLAB command "ctrb" was used to perform this verification showing that there is no uncontrollable mode; therefore, the pair $(\boldsymbol{A}, \boldsymbol{B})$ is stabilizable. As ρ, σ_D, and σ_V are strictly positive constants, matrices $\boldsymbol{R}$ and $\boldsymbol{Q}$ are positive definite. Then it can be concluded that all of the criteria are fulfilled, and thus an LQR controller can stabilize the system.

Nonlinear Method

Lyapunov Function

A nonlinear approach was also studied in an effort to improve the performance of the system. Before the analysis, the variables that were used in the development of this controller were defined as

$$\boldsymbol{r} = [x \quad y \quad z]^T, \qquad \boldsymbol{v} = [\dot{x} \quad \dot{y} \quad \dot{z}]^T$$

These six parameters define the absolute position and the velocity of the satellite under consideration (and not the relative position and velocity as had been defined for the LQR controller).

The stability of the system, which can be represented by the simple form $\dot{\boldsymbol{z}} = f(\boldsymbol{z})$, is analyzed using Lyapunov's stability approach by constructing a scalar Lyapunov function of the state $V(z)$. For this type of system, the equilibrium point is globally asymptotically stable if there is a function $V(z)$ continuous in the first derivative that satisfies the following conditions:

$$V(0) = 0, \qquad V(\boldsymbol{z}) > 0 \,\forall\, \boldsymbol{z} \neq 0$$
$$\dot{V}(\boldsymbol{z}) < 0 \,\forall\, \boldsymbol{z} \neq 0, \qquad \lim_{|z| \to \infty} V = \infty \tag{10}$$

No method guaranteed to generate Lyapunov functions exists, but quadratic and logarithmic forms are often effective starting points in a trial-and-error approach.

The state vector $\boldsymbol{X}(t)$ is defined as

$$\boldsymbol{X}(t) = [\delta x \quad \delta y \quad \delta z \quad \delta \dot{x} \quad \delta \dot{y} \quad \delta \dot{z}]^T \tag{11}$$

which corresponds to the difference between the actual position and velocity of the follower and its desired position and velocity. The chosen function must be positive definite so that its derivative about $\boldsymbol{X}(t)$ is only negative for decreasing state vector magnitudes and is given by

$$V(\delta \boldsymbol{r}, \delta \boldsymbol{v}) = \tfrac{1}{2} k_1 \delta \boldsymbol{r}^T \delta \boldsymbol{r} + \tfrac{1}{2} k_2 \delta \boldsymbol{v}^T \delta \boldsymbol{v} \tag{12}$$

where k_1 and k_2 are positive gains.

From this choice, the time derivative of the Lyapunov function V can be obtained as

$$\dot{V}(\delta \boldsymbol{r}, \delta \boldsymbol{v}) = [k_1 \delta \boldsymbol{r} + k_2 \delta \boldsymbol{v}]^T \delta \boldsymbol{f} \tag{13a}$$

with

$$\delta \boldsymbol{f} = \begin{bmatrix} \delta \dot{\boldsymbol{r}} \\ \delta \ddot{\boldsymbol{r}} \end{bmatrix} = \begin{bmatrix} \delta \boldsymbol{v} \\ \ddot{\boldsymbol{r}} - \ddot{\boldsymbol{r}}_{\text{ref}} + \boldsymbol{u} \end{bmatrix} \tag{13b}$$

State Feedback Linearization

The selected controller is based on a state-feedback-linearization technique. The intent of this approach is to cancel the nonlinear dynamics and to impose a desired linear form instead. To define the acceleration vector of the follower, a compromise between accuracy and complexity has been made. Thus, Earth oblateness is the only perturbation included in the controller logic. The acceleration vector is then given by the expression

$$\ddot{\boldsymbol{r}} = -\mu_{\text{earth}} \left\{ \frac{\boldsymbol{r}}{r^3} + J_2 R_{\text{Earth}}^2 \left[\frac{3z}{r^5} \boldsymbol{e}_3 + \frac{3}{2} \left(1 - 5 \frac{z^2}{r^2} \right) \frac{\boldsymbol{r}}{r^5} \right] \right\} \tag{14}$$

The relative acceleration vector can then be represented by the expression

$$\ddot{\boldsymbol{r}} - \ddot{\boldsymbol{r}}_{\text{ref}} = -\mu_{\text{earth}} \left\{ \left(\frac{\boldsymbol{r}}{r^3} - \frac{\boldsymbol{r}_{\text{ref}}}{r_{\text{ref}}^3} \right) + J_2 R_{\text{Earth}}^2 \left[\left(\frac{3z}{r^5} - \frac{3z_{\text{ref}}}{r_{\text{ref}}^5} \right) \boldsymbol{e}_3 + \frac{3}{2} \left(1 - 5 \frac{z^2}{r^2} \right) \frac{\boldsymbol{r}}{r^5} - \frac{3}{2} \left(1 - 5 \frac{z_{\text{ref}}^2}{r_{\text{ref}}^2} \right) \frac{\boldsymbol{r}_{\text{ref}}}{r_{\text{ref}}^5} \right] \right\} \tag{15}$$

The next step is to define the control acceleration law that cancels the position error and the relative acceleration vector, and that satisfies the criteria of asymptotic stability. The selected law that matches all of the criteria is given by

$$\boldsymbol{u}_{\text{Lyap}} = \mu_{\text{earth}} \left\{ \left(\frac{\boldsymbol{r}}{r^3} - \frac{\boldsymbol{r}_{\text{ref}}}{r_{\text{ref}}^3} \right) + J_2 R_{\text{Earth}}^2 \left[\left(\frac{3z}{r^5} - \frac{3z_{\text{ref}}}{r_{\text{ref}}^5} \right) \boldsymbol{e}_3 + \frac{3}{2} \left(1 - 5 \frac{z^2}{r^2} \right) \frac{\boldsymbol{r}}{r^5} - \frac{3}{2} \left(1 - 5 \frac{z_{\text{ref}}^2}{r_{\text{ref}}^2} \right) \frac{\boldsymbol{r}_{\text{ref}}}{r_{\text{ref}}^5} \right] \right\} - \frac{k_1}{k_2} \delta \boldsymbol{r} - k_3 \delta \boldsymbol{v} \tag{16}$$

If the Lyapunov control law $\boldsymbol{u}_{\text{Lyap}}$ is substituted into $\delta \boldsymbol{f}$, it can be observed that the time derivative of the Lyapunov function is negative:

$$\dot{V}(\delta \boldsymbol{r}, \delta \boldsymbol{v}) = -k_2 k_3 \delta \boldsymbol{v}^T \delta \boldsymbol{v} \tag{17}$$

Note that Eq. (17) depends only on $\boldsymbol{v}$, and global asymptotic stability cannot be proven as $\dot{V}$ might be equal to zero at $\delta \boldsymbol{r} \neq 0$. However, as $\delta \dot{\boldsymbol{r}} = \delta \boldsymbol{v}$, and $\delta \dot{\boldsymbol{v}} = -(k_1/k_2)\delta \boldsymbol{r} - k_3 \delta \boldsymbol{v}$, $\delta \boldsymbol{v} = 0$, and $\delta \dot{\boldsymbol{v}} = 0$ imply $\delta \boldsymbol{r} = 0$ as well. Thus, the largest set where $\dot{V}$ is equal to zero includes only the origin. Therefore, LaSalle's invariance principle can be applied. As the function V tends to infinity when $\|\boldsymbol{x}\|$ tends to infinity, then V is radially unbounded. Therefore, it can be stated that the system is globally asymptotically stable under the control given by Eq. (16).

The Lyapunov control law can be subdivided into three separate parts: the dynamic part, the proportional part, and the derivative part (as $\delta \boldsymbol{v} = \delta \dot{\boldsymbol{r}}$) and can be expressed as

$$\boldsymbol{u}_{\text{Lyap}} = \mu_{\text{Earth}} \left\{ \left(\frac{\boldsymbol{r}}{r^3} - \frac{\boldsymbol{r}_{\text{ref}}}{r_{\text{ref}}^3} \right) + J_2 R_{\text{Earth}}^2 \left[\left(\frac{3z}{r^5} - \frac{3z_{\text{ref}}}{r_{\text{ref}}^5} \right) \boldsymbol{e}_3 + \frac{3}{2} \left(1 - 5 \frac{z^2}{r^2} \right) \frac{\boldsymbol{r}}{r^5} - \frac{3}{2} \left(1 - 5 \frac{z_{\text{ref}}^2}{r_{\text{ref}}^2} \right) \frac{\boldsymbol{r}_{\text{ref}}}{r_{\text{ref}}^5} \right] \right\} + K_{\text{global}} \left(\frac{-K_P \delta \boldsymbol{r} - K_D \delta \boldsymbol{v}}{\| K_P \delta \boldsymbol{r} + K_D \delta \boldsymbol{v} \|} \right) \tag{18}$$

The gain K_{global} has been introduced to maintain the desired ratio between proportional and derivative gains when the overall scaling

factor varies. As only proportional and derivative components of the controller have associated gains, asymptotic stability is guaranteed only when the entire dynamic component is applied. If the dynamic component becomes so large so that the available amount of thrust is not sufficient to correct it, the system can no longer be stabilized with the given propulsion system capability.

Simulator Architecture

To simulate the motion of each spacecraft, a model was developed using MATLAB. The following perturbations were implemented in this model: 1) Earth geopotential of degree and order 30 based on Goddard Earth Model T1; 2) solar and lunar gravity perturbations modeled using series expansions of ephemerides[11] to locate the sun and moon, where these expansions are accurate to about 0.1–1%; 3) solar radiation pressure assuming that both satellites continuously receive full illumination from the sun (no eclipse) and using the ephemerides mentioned earlier to compute the position of the sun relative to the Earth; and 4) atmospheric drag based on the Harris–Priester atmospheric density model and a worst-case drag coefficient of 2.2.

A model with higher fidelity is currently under development and will be used in future efforts to further validate the results presented here (although some validation has been done as detailed next).

In this initial study, it was assumed that the feedback dynamic is instantaneous: that the measurements of the leader/follower's positions and velocities are instantaneously transmitted to the onboard computer and processed immediately. However, real systems will encounter delays. The effects of these delays will be a topic of future study.

To propagate the equations of motion related to each spacecraft, a seventh- to eighth-order variable step-size Runge–Kutta technique with an error tolerance of 10^{-9} was used. The state of each spacecraft was propagated independently of the other, and then their relative velocities were computed. The time step for the controller was arbitrarily set as 2 s. Every 2 s, the relative position and velocity of the leader (compared to the follower) are computed, and the appropriate command is issued by the controller (firing the thrusters or not and direction of the burn if firing). The command is then applied for the next 2 s (regardless of what occurs during this 2-s interval). Note that the simulator accounts for the changing mass of the follower as the propellant is consumed. The model developed to simulate the changing mass of the follower is linear because the selected engine has a constant fuel rate (new mass equals previous mass minus fuel flow rate times firing duration).

To verify that the model developed is accurate, comparisons were made with the NASA/Jet Propulsion Laboratory software POHOP. Atmospheric drag, solar radiation pressure, and lunar/solar gravitational effects were used with the Earth geopotential set to degree and order six. The values of the leader/follower Cartesian components in the terrestrial frame were recorded after 12 h of free drift as computed by each code and are shown in Table 1. Note that the percent error on the follower's coordinates is very close to the percent error on the leader's coordinates. Because the relative position of the spacecraft is the main interest of this study, the differences are deemed sufficiently small for the level of accuracies required in this initial study.

Constant Thrust Constraint

Because the thrusters are assumed to not have variable thrust capability (on-off engines only), they will be used only when the amount of impulse requested by the controller equals or exceeds the available amount of thrust. The requested amount of thrust is defined by the control law and depends on the relative position and the relative velocity. The available amount of acceleration is computed using

$$\text{available acceleration} = (T/m) \tag{19}$$

Table 1 Percent error of each Cartesian coordinate at 12 h

Spacecraft	x	y	z	$\dot{x}$	$\dot{y}$	$\dot{z}$
Follower, %	0.3943	−0.0642	−0.0366	−0.0351	0.4822	0.3678
Leader, %	0.3946	−0.0642	−0.0366	−0.0351	0.4825	0.3681

Results

To determine effective values for weights and gains defining each controller, a large number of simulations were conducted in a trial-and-error process. Table 2 presents the ranges over which each variable was evaluated.

For the LQR controller, this trial-and error process showed that a tradeoff must be made between very high performances (in terms of relative position and relative velocity control) and propellant consumption. As propellant consumption is a main criterion for most missions, a high scalar control weighting factor is preferable. In regards to the nonlinear controller, changing the gains only impacts the accuracy because this controller induces continuous thrusting regardless of the gain values. The best values identified for the weights and gains of the linear and the nonlinear controllers are given in Table 3.

Nominal Chase

In this section, it is assumed that the bielliptic transfer has been successfully performed and that mission is in the continuous chasing phase. This assumption affects the initial conditions entered in the MATLAB code. At $t = 0$, the follower is at the desired point at 10 m behind the leader and on the same orbit. Figures 4 and 5 present the spacecraft separation obtained with the linear controller and with the nonlinear controller, respectively (initial altitude of 700 km).

An accuracy of plus or minus 3 cm was obtained with the linear controller compared to an accuracy of plus or minus 3 mm with the nonlinear controller. However, propellant consumption with the

Table 2 Trial-and-error ranges

Linear controller	Nonlinear controller
ρ: [1,000:50,000]	K_{global}: [0.01:1,000]
——	K_D/K_P: [1:10]

Table 3 Main parameters and primary assumptions made for the two controllers

Linear controller	Nonlinear controller
No perturbation included in the controller	Earth oblateness effects included in the controller
Circular orbits assumed	Noncircular orbits
$\rho = 50{,}000$	$K_{\text{global}} = 10$
$\sigma_D = 1$	$K_P = 1$
$\sigma_V = 1$	$K_D = 10$

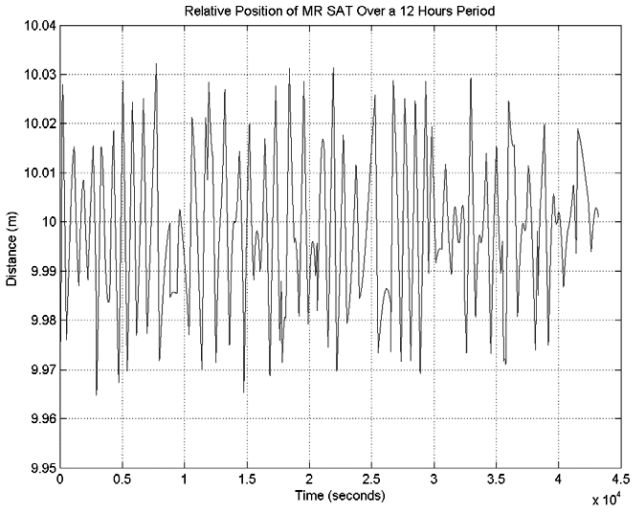

Fig. 4 Spacecraft separation with linear controller (no noise).

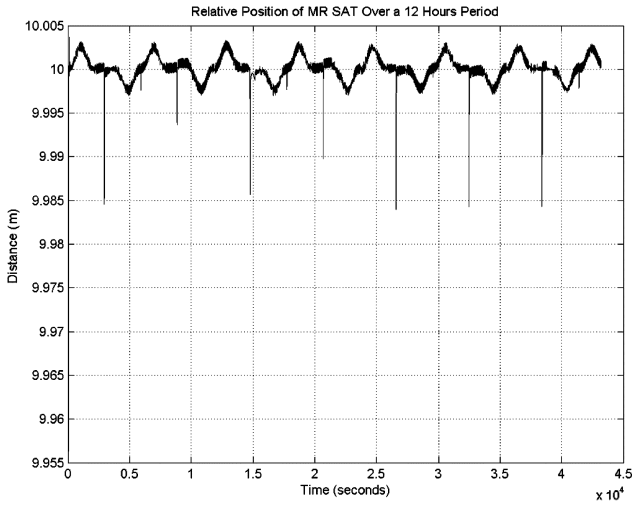

Fig. 5 Spacecraft separation with nonlinear controller (no noise).

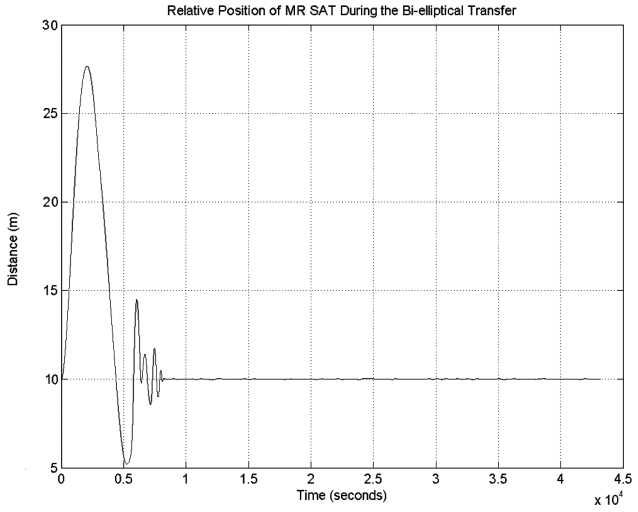

Fig. 6 Bielliptic transfer with linear controller (no noise).

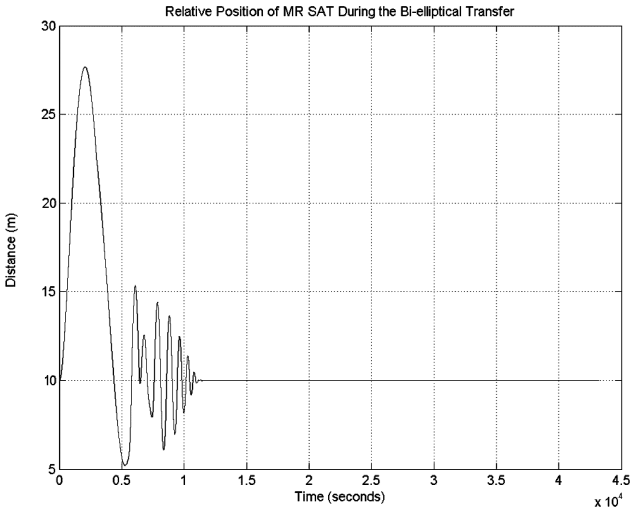

Fig. 7 Bielliptic transfer with nonlinear controller (no noise).

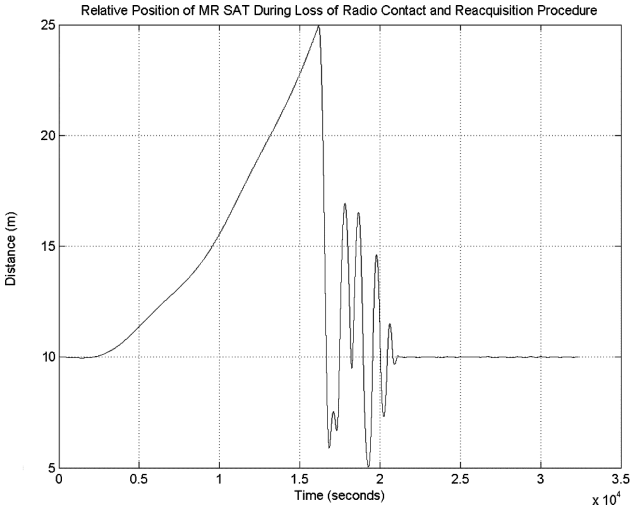

Fig. 8 Loss of radio contact with linear controller (no noise).

nonlinear controller is much larger as it requires continuous thrusting to achieve this level of accuracy. Note that these simulations do not guarantee such levels of accuracy as perturbations on the order of centimeters have been omitted in the simulator (including radiation pressure from the Earth, tidal forces, relativistic effects, and empirical forces). Therefore, a more precise simulator is needed to determine the actual level of accuracy. However, these simulations suggest satisfactory controllability for the goals of the MR SAT project.

Bielliptic Transfer

Only the first two burns (of the three) that compose the bielliptic transfer will be performed. The last one will be replaced by activating the control system to ensure a precise 10-m separation at the end of the procedure. The activation takes place at $t = 5500$ s. At initiation of the transfer ($t = 0$), the follower is located 10 m "below" the leader along the radial direction on a different orbit (i.e., a slightly lower orbit). Figures 6 and 7 present the spacecraft separation obtained with the linear controller and with the nonlinear controller, respectively.

In these figures, the first maneuver is performed at $t = 0$ and the second at $t = 2963$ s. These two figures show that both controllers successfully stabilize the follower at the desired position. Note that the system is stabilized more quickly with the linear controller. Also note that the relative separation remains within the 460-m range of the wireless communication system throughout the entire transfer.

Loss of Radio Contact and Reacquisition

A scenario was simulated to check the ability of the system to restabilize itself in the event intersatellite communications were lost for a limited amount of time (approximately $4\frac{1}{2}$ h in this example). Figures 8 and 9 present the spacecraft separation obtained with the linear controller and with the nonlinear controller, respectively.

These two figures show that both controllers successfully restabilize the follower at the desired position after a loss of radio contact, as long as the loss of contact is sufficiently short. At an altitude of 700 km, the system cannot be restabilized when the drift between the two spacecraft exceeds 35 m before radio contact is restored. The cause of this instability is the low level of thrust available, as the propulsion system is assumed to deliver only 3.062 mn of thrust. If the dynamics of the system is "stronger" than the control system, stability cannot be achieved. Note that this maximum distance for which the controller cannot restabilize the system depends on the altitude of the formation. The atmospheric drag is the main cause for the formation to destabilize and of course increases as altitude decreases.

Simulations Including Measurement Noise

Measurement noise will occur during the mission and the magnitude of these errors will depend on the orbit and attitude determination techniques used by the onboard computers. This measurement noise will have a significant impact on the performance of the entire system and must be taken into consideration during the design/simulation process. The magnitude of this measurement

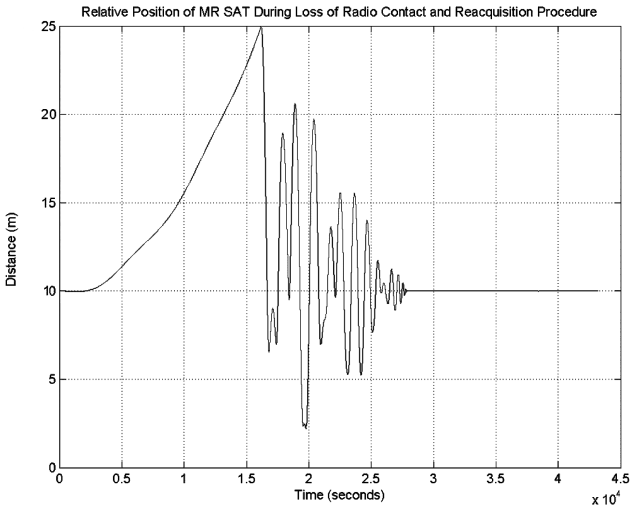

Fig. 9 Loss of radio contact with nonlinear controller (no noise).

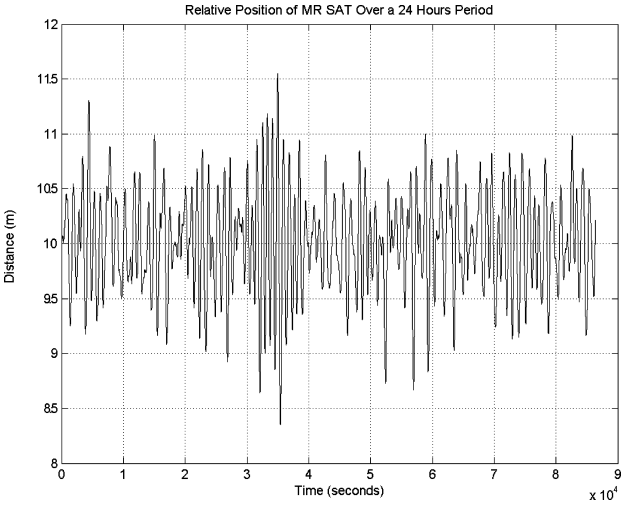

Fig. 10 Spacecraft separation with linear controller (with noise).

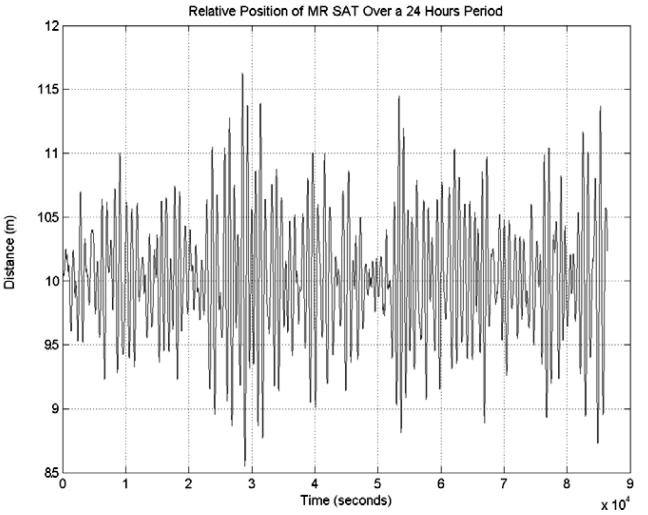

Fig. 11 Spacecraft separation with nonlinear controller (with noise).

noise was estimated as follows: 1) position error, random (Gaussian) up to 1 m along each axis (in the Earth-fixed frame); 2) velocity error, random (Gaussian) up to 0.1 m/s along each axis (in the Earth-fixed frame); and 3) attitude error, random (Gaussian) up to 2.5 deg along each axis, as determined by magnetometers (in the local vertical local horizontal frame).

Note that the magnitudes of these errors include the effects of postprocessing techniques performed by the onboard computer to improve the accuracy of the raw GPS data. The control system will not be fed with "raw" GPS data, but with "corrected" GPS data. For example, because both satellites will be in close proximity, their absolute positions will be nearly equally affected by GPS errors. These errors can be virtually eliminated by postprocessing techniques applied in near real time by the onboard computer, increasing the accuracy of the relative position. These postprocessing techniques will be required in order to achieve the mission objectives (in terms of separation) because the accuracy of GPS receivers is significantly lower than the presented error values. The estimated errors were taken from potential postprocessing techniques that could be used in small satellite applications. These techniques are not presented in this paper.

The consequences of these noise measurements are a decrease in accuracy of formation control and a significant increase of the propellant consumption. With the measurement noise taken into consideration, both the linear and the nonlinear controller perform continuous thrusting to achieve the required accuracy. Only the nominal chase mode was simulated with the measurement noise included. Figures 10 and 11, respectively, present the spacecraft separation obtained with the linear controller and with the nonlinear controller (an initial altitude of 700 km).

These two figures show that both controllers can stabilize the system under these perturbed conditions. An accuracy within 1.5 m was obtained with both controllers, which roughly corresponds to the measurement noise. Both controllers now require continuous thrusting to stabilize the system.

To evaluate the behavior of the two controllers with less sophisticated postprocessing techniques, simulations were also conducted with larger measurement noises. Note that with velocity errors of ± 1 m/s along each axis, the linear controller with the already defined set of parameters is no longer stable, and only the nonlinear controller can stabilize the system under these conditions. This phenomenon illustrates the higher robustness of a nonlinear controller over a linear controller.

Controller Enhancement to Reduce Propellant Consumption

Continuous thrusting implies a propellant consumption of 407 g per day, which gives a mission lifetime of 35 h. To increase the lifetime of the mission, it was decided to decrease the requirements in terms of formation geometry from plus or minus 1 m to plus 10 m, minus 5 m, and to add a specific conditional check in each controller: the stability of the system is now constantly monitored. The system is considered stabilized if the distance between the two satellites is in the interval [9–11] (meters) for more than 1500 s. When the system is stabilized, the controller is turned off until the distance between the follower and the leader reaches 15 m or goes below 7 m. Then the controller is turned back on until the system is restabilized. This specific procedure is only applied during the nominal chase mode, and not during the other phases of the mission. Figures 12 and 13 present the spacecraft separation obtained with the linear controller and with the nonlinear controller, respectively (at an initial altitude of 700 km).

By adding this subroutine, propellant consumption is reduced by 20% for the linear controller and by 15% for the nonlinear controller. However, consumption remains high, and an increase of the quantity of onboard propellant is still required to meet the objective of conducting the chase phase for two weeks. Propellant consumption remains lower with the linear controller as it is based on an optimal design (LQR) with a very high weight on propellant usage.

Sensitivity of the System to Altitude Changes

Simulations over 12 h were performed to evaluate the controller sensitivity to other possible initial altitudes. These initial altitudes were arbitrarily selected as 400 and 300 km. Results show that both controllers stabilize the system at these two altitudes. Because of space limitations, only the results at 300 km are presented in Figs. 14 and 15.

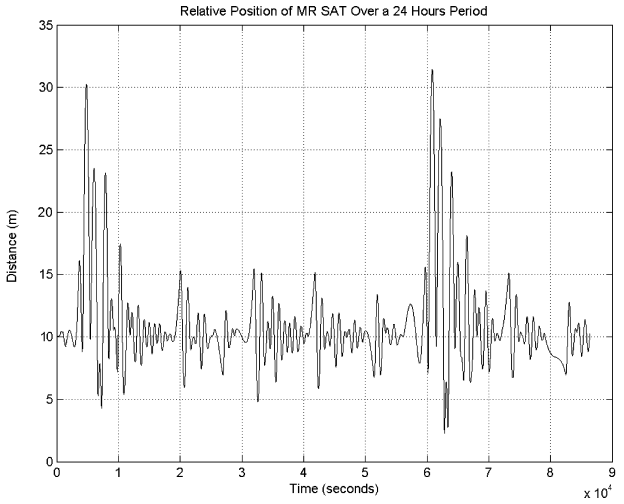

Fig. 12 Spacecraft separation with enhanced linear controller (with noise).

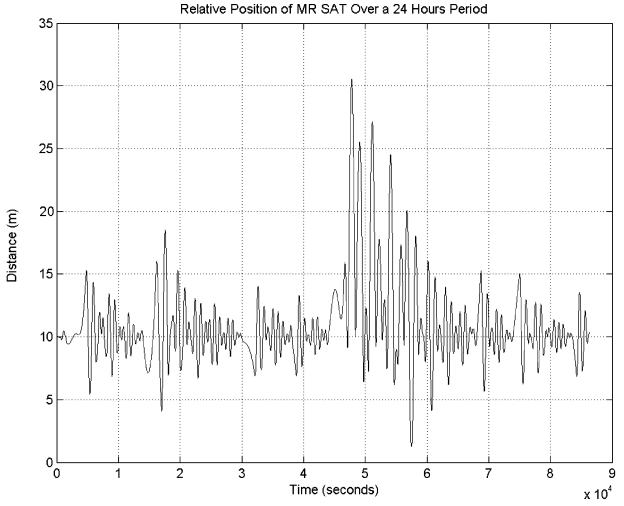

Fig. 13 Spacecraft separation with enhanced nonlinear controller (with noise).

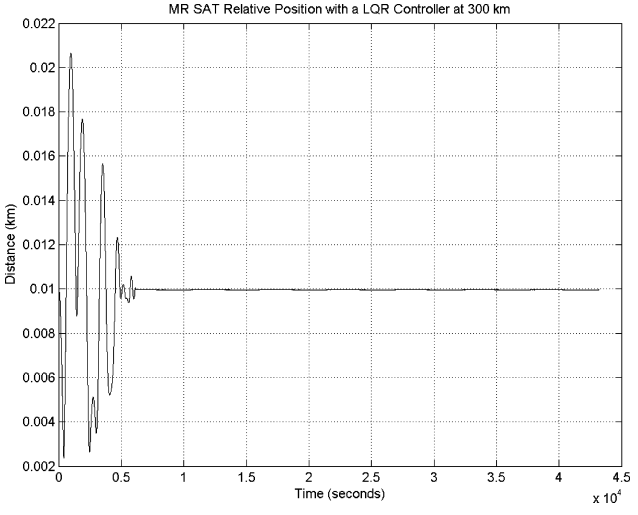

Fig. 14 Nominal chase with LQR controller at 300 km (no noise).

Table 4 Performance summary

Orbit	Linear controller	Nonlinear controller
Nominal chase at 700 km	3.58 g/day	118.57 g/day
Nominal chase at 400 km	12.96 g/day	184.28 g/day
Nominal chase at 300 km	105.72 g/day	326.94 g/day
Bielliptical transfer	13.19 g	29.11 g

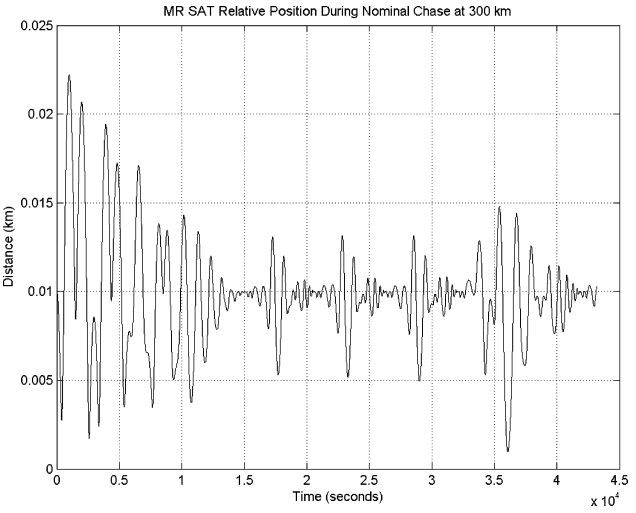

Fig. 15 Nominal chase with enhanced Lyapunov controller at 300 km (no noise).

Performance Summary

A key metric of the chasing process is the propellant consumption. Propellant consumption of the linear and nonlinear controllers are summarized in Table 4. The propellant consumption corresponds to the three initial altitudes previously considered (300, 400, and 700 km) and to the different phases of the mission. Note that for the nominal chase mode the values in Table 4 correspond to the enhanced Lyapunov controller. Results are presented in grams.

Safe Mode of Operation

In case of a significant loss of radio contact, the distance between the spacecraft will exceed the maximum stabilizable range of the controller (35 m). However, by using the leader's last known coordinates (position and velocity), its trajectory can be propagated, and the follower can then track this predicted trajectory to remain within the stabilizable range and be prepared to resume nominal Chase mode when the radio signal is reacquired. During the nominal chase mode, frequent radio contact checks are performed. As long as the follower receives data from the leader, the active control system remains in the nominal chase mode. However, if a loss of radio contact is detected, the nominal chasing procedure is suspended, and the following procedure is applied instead:

1) The last known data from the leader are recorded.

2) The leader's future position and velocity are simulated onboard the follower. From these theoretical values, the relative position and the relative velocity of the follower are computed.

3) When the theoretical distance between the two spacecraft exceeds 30 m, the controller is reactivated and is provided with the simulated data until the system is restabilized (distance of 10 m plus or minus 30 cm maintained for more than 2000 s). The reactivation distance for this procedure was selected to be 30 m in order to avoid collision and to provide a small safety margin regarding the maximum allowable distance of 35 m. Because the position of the leader is no longer precisely known, the standard 15-m reactivation distance is too short.

4) The controller is then turned off until the theoretical distance exceeds 30 m again.

5) The procedure is repeated until the loss of radio contact duration reaches a certain value. For a given model, this duration depends

on the altitude at which the loss of radio contact occurred, at which point the chasing process is terminated. Further actions can be decided by the ground crew based on the current situation.

Obviously, the more accurate the model, the longer the process can attempt reacquisition. It is added that, if at any time during the loss of radio contact, the signal is reacquired, and the system switches back to the nominal mode immediately. Checks for radio signal reacquisition are performed independently from this procedure every 30 s.

A key parameter of this procedure is the accuracy of the estimating process. Computational power capability is directly linked to the complexity of the model that can be implemented into the onboard computer. The model implemented can vary from a simple orbit equation (assuming no perturbations) to the full MATLAB model developed for this study (with numerical integration of the differential equations). The complexity of the model can be selected based on the computational power of the onboard computer. However, the simple orbit equation can provide adequate results if the radio contact is not lost for an excessively long time period.

Conclusions

This study shows that for low-Earth-orbit activities, a Clohessy–Wiltshire linearization used with linear-quadratic-regulator control can provide adequate control accuracy for formations composed of microsatellites as long as the uncertainties (measurement noise, etc.) remain limited. If the uncertainties are known to be within prescribed limits, the linear controller appears to be the best suited because of its high performance with regards to propellant consumption. As uncertainties grow, the difference in terms of propellant consumption between the linear and the nonlinear controllers decreases. Ultimately, the linear controller will become unstable when it encounters sufficiently large uncertainties (such as velocity errors greater than ± 1 m/s along each axis), whereas the nonlinear controller will still stabilize the system. Therefore, for systems with large measurement noise, switching to a nonlinear controller is required to ensure stability of the system. In this case, the overall complexity of the controller is significantly increased, but the robustness of the system is also significantly increased. Therefore, the final choice between a linear and a nonlinear controller must be made based on the level of expected uncertainties on each mission's parameters and also regarding the range of these parameters. In the cases considered in this study, the nonlinear Lyapunov-based controller is the best suited. The original goal of a 10-m separation (plus or minus 1 m) was achieved with the developed controllers. Formation control accuracies varied according to the order of magnitude of the measurement noise. Regarding propellant consumption, the original goal was achieved with the two controllers presented in this paper, but only by slightly downgrading the maximum allowable separation distance.

Because of the low level of thrust assumed available onboard the follower spacecraft, intersatellite communication is critical and cannot be lost for more than a couple of hours. Furthermore, this low level of available thrust strongly limits the capabilities of the system in terms of formation geometry.

References

[1]Kapila, V., Sparks, A. G., Buffington, J. M., and Yan, Q., "Spacecraft Formation Flying: Dynamics and Control," *Journal of Guidance, Control, and Dynamics*, Vol. 23, No. 3, 2000, pp. 561–564.

[2]Starin, S. R., Yedavalli, R. K., and Sparks, A. G., "Spacecraft Formation Flying Maneuvers Using Linear-Quadratic Regulation with No Radial Axis Input," AIAA Paper 2001-4029, Aug. 2001.

[3]Starin, S. R., Yedavalli, R. K., and Sparks, A. G., "Design of a LQR Controller of Reduced Inputs for Multiple Spacecraft Formation Flying," *Proceedings of the American Control Conference*, Vol. 2, 2001, pp. 1327–1332.

[4]Chattergy, R., "Stability of Nonlinear Motions of a Satellite," *Proceedings of the American Control Conference*, Vol. 5, 1995, pp. 3620, 3621.

[5]Sparks, A. G., "Satellite Formationkeeping Control in the Presence of Gravity Perturbations," *Proceedings of the American Control Conference*, Vol. 2, 2000, pp. 844–848.

[6]Yan, Q., Yang, G., Kapila, V., and de Queiroz, M. S., "Nonlinear Dynamics and Output Feedback Control of Multiple Spacecraft in Elliptical Orbits," *Proceedings of the American Control Conference*, Vol. 2, 2000, pp. 839–843.

[7]Wang, Z., Khorrami, F., and Grossman, W., "Robust Adaptive Control of Formationkeeping for a Pair of Satellites," *Proceedings of the American Control Conference*, Vol. 2, 2000, pp. 834–838.

[8]Naasz, B. J., "Classical Element Feedback Control for Spacecraft Orbital Maneuvers," M.S. Thesis, Aerospace Engineering Dept., Virginia Polytechnic Inst. and State Univ., Blacksburg, VA, May 2002.

[9]Gurfil, P., Idan, M., and Kasdin, J. N., "Neurocontrol of Spacecraft Formation Flying in the Elliptic Restricted Three-Body Problem," *Journal of Guidance, Control, and Dynamics*, Vol. 26, No. 3, 2003, pp. 491–501; also AIAA Paper 2002-4962, Aug. 2002.

[10]Nelson, E., Sparks, A., and Kang, W., "Coordinated Nonlinear Tracking Control for Satellite Formations," AIAA Paper 2001-4025, Aug. 2001.

[11]Montenbruck, O., and Gill, E., "Low-Precision Solar and Lunar Coordinates," *Satellite Orbits: Models, Methods, and Applications*, 1st ed., Springer-Verlag, Berlin, 2000, pp. 70–73.

C. McLaughlin
Associate Editor